doi:10.1006/jmbi.2001.4764 available online at http://www.idealibrary.com on IDEAL® *J. Mol. Biol.* (2001) **310**, 219–230

JMB

Solution Structure of Human IL-13 and Implication for Receptor Binding

Franklin J. Moy[1], Elizabeth Diblasio[2], James Wilhelm[1] and Robert Powers[1]*

[1]*Department of Biological Chemistry*

[2]*Department of Genomics Wyeth Research, 87 Cambridge Park Drive, Cambridge MA 02140, USA*

**Corresponding author*

Interleukin-13 has been implicated as a key factor in asthma, allergy, atopy and inflammatory response, establishing the protein as a valuable therapeutic target. The high-resolution solution structure of human IL-13 has been determined by multidimensional NMR. The resulting structure is consistent with previous short-chain left-handed four-helix bundles, where a significant similarity in the folding topology between IL-13 and IL-4 was observed. IL-13 shares a significant overlap in biological function with IL-4, a result of the common α chain component (IL-4Rα) in their respective receptors. Based on the available structural and mutational data, an IL-13/IL-4Rα model and a sequential mechanism for forming the signaling heterodimer is proposed for IL-13.

Keywords: NMR; solution structure; interleukin-13; interleukin-4

Introduction

Interleukin-13 (IL-13) is a pleiotropic cytokine with roles in atopy, asthma, allergy and inflammatory response.[1–5] IL-13 is produced by activated T-cells and promotes B-cell proliferation, induces B-cells to produce IgE, down-regulates the production of proinflamatory cytokines, increases expression of VCAM-1 on endothelial cells, enhances the expression of class II MHC antigens and various adhesion molecules on monocytes. IL-13 mediates these functions through an interaction with its receptor on hematopoietic and other cell types, but currently no functional receptors have been identified on T-cells. The signaling human IL-13 receptor (IL-13R) is a heterodimer composed of the interleukin-4 receptor α chain (IL-4Rα) and the IL-13 binding chain. Two IL-13 binding chains that are 27% homologous have been identified, IL-13Rα1 and IL-13Rα2. IL-13Rα2 demonstrates an approximate 100-fold higher affinity for IL-13 relative to IL-13Rα1 in the absence of IL-4Rα, but has been identified only in the serum and urine of mice. The association of IL-13 with its receptor induces the activation of STAT6 (signal transducer and activation of transcription 6) and Janus-family kinase (JAK1, JAK2, TYK2) through a binding interaction with the IL-4Rα chain.

IL-13 is located in a cluster of genes on chromosome 5 encoding IL-3, IL-4, IL-5, IL-9 and GM-CSF. IL-13 shares many functional properties with IL-4 as a result of the common IL-4Rα component in their receptors.[6,7] IL-4 exhibits a high affinity to the IL-4Rα chain (K_d = 20-300 pM), where this complex recruits the common γ chain (γ_c) of IL-4R to form the signaling complex. Similarly, IL-13 binds to the IL-13 binding chain (IL-13Rα1) with relatively high affinity ($K_d \sim 4$ nM) in the absence of the IL-4Rα chain, where an increase in affinity to IL-4R occurs in the presence of IL-4Rα (K_d = 50 pM). IL-13 does not bind IL-4Rα in the absence of the IL-13 binding chain. As a result, IL-4 exhibits binding to both IL-4R and IL-13R due to the existence of the IL-4Rα chain in both receptors, but IL-13 does not bind IL-4R because of the absence of the IL-13 binding chain.[6] The cross-reactivity of IL-4 with both IL-4R and IL-13R is further promoted by the antagonistic activity of the IL-4 Y124D mutant.[8] The IL-4 Y124D mutant still maintains the ability to bind IL-4Rα, but is deficient in its ability to induce a signal through interaction with the γ_c chain. Since the γ_c chain is not present in IL-13R, IL-13 does not induce the proliferation and

Abbreviations used: IL-13, interleukin-13; IL-4, interleukin-4; IL-13R, interleukin-13 receptor; IL-4R, interleukin-4 receptor; IL-4Rα, interleukin-4 receptor α chain; IL-13R-BC, interleukin-13 receptor binding chain, γ_c, IL-4 receptor common γ chain; HMQC, heteronuclear multiple-quantum coherence spectroscopy; NOE, nuclear Overhauser effect; NOESY, nuclear Overhauser enhanced spectroscopy; COSY, correlated spectroscopy.

E-mail address of the corresponding author: powersr@war.wyeth.com

0022-2836/01/010219–12 $35.00/0

differentiation of T-cells or the activation of JAK-3 kinase, which associates with the γ_c chain of IL-4R.

IL-13 and IL-4 are both members of the short-chain four-helix bundle cytokine family,[9] where both solution and crystal structures have been determined for IL-4.[10–14] Despite the relatively low (25 %) sequence homology between IL-13 and IL-4, a similarity in the overall topology between the two proteins is expected. A combination of mutational and kinetic analysis has identified a distinct site on the IL-4 structure associated with IL-4Rα binding and a second site associated with signaling through the γ_c chain.[15–17] Recently, the X-ray structure of IL-4 complexed with the ectodomain of IL-4Rα has been determined, which further defines the IL-4 - IL-4Rα interface.[18]

Despite the abundance of structural information on the IL-4 receptor system, structural information for IL-13, IL-13R or the complex is currently lacking. To further our understanding of the IL-13 receptor system and as part of a structure-based drug design program, we have determined the high-resolution solution structure of human IL-13 by heteronuclear multidimensional NMR. Furthermore, since IL-13 and IL-4 are structural homologs, correlation of the mutational data for both IL-4 and IL-13 with the structure of the IL-4-IL-4Rα complex and the solution structure of IL-13 described herein may provide insight into the IL-13-IL13R complex.

Results and Discussion

IL-13 NMR structure

Nearly complete backbone and side-chain ^{1}H, ^{15}N, ^{13}C, and ^{13}CO assignments have been obtained for IL-13 that enabled the determination of a high-resolution solution structure for the protein by NMR (Figure 1). The IL-13 structure is well defined by the NMR data, where a total of 2848

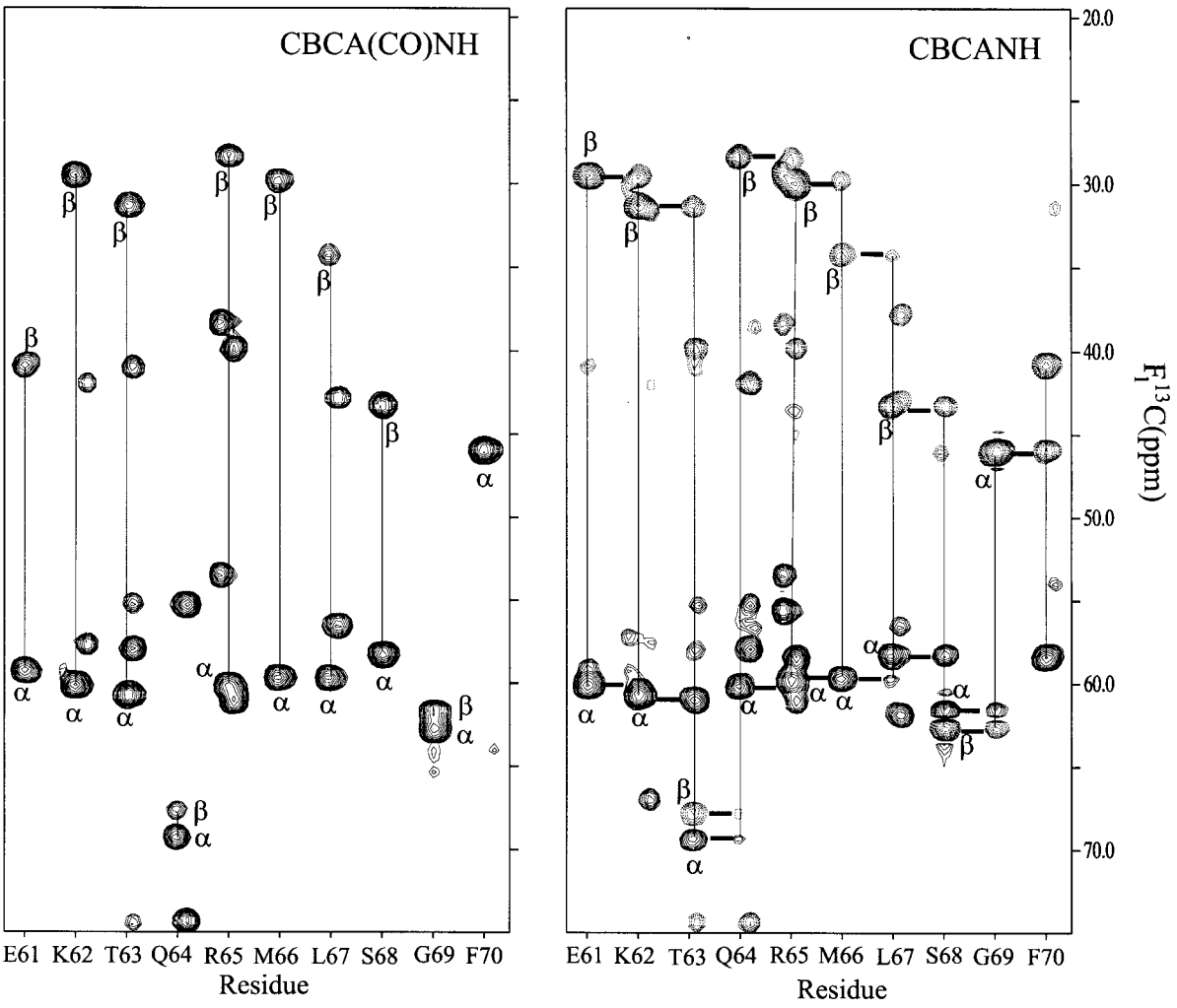

Figure 1. Strip plots taken from the CBCA(CO)NH and CBCANH spectra for the amide groups of residues E61 through F70 of IL-13. Each amide group correlates with the C^α and C^β of the preceding residue in the CBCA(CO)NH spectra and with both its intraresidue C^α and C^β, and the C^α and C^β of the preceding residue in the CBCANH spectra. Interresidue $(i-1)$ correlations are labeled where the observed interresidue connectivities are markedly thick lines. The correlations associated with a particular amide group are connected with a thin line.

constraints were used to refine the structure (Figure 2). This is evident by a best-fit superposition of the backbone atoms shown in Figure 3, where the atomic r.m.s. distribution of the 30 simulated annealing structures about the mean coordinate positions for residues 1-113 is 0.43(±0.04) Å for the backbone atoms (Table 1). All of the backbone torsion angles for non-glycine residues lie within expected regions of the Ramachandran plot, where 89.9 % of the residues lie within the most-favored region of the Ramachandran ϕ,ψ plot, 9.1 % in the additionally allowed region and 1.0 % in the generously allowed region. The high quality of the IL-13 NMR structure is evident also by the results of the PROCHECK analysis, where an overall *G*-factor of 0.15, a hydrogen bond energy of 0.90 and only 1.8 bad contacts per 100 residues were determined. The calculated PROCHECK parameters for IL-13 are comparable to values obtainable with ~1 Å X-ray structures and imply a relatively high quality for the structure, but does not infer an inherent resolution.[19]

The IL-13 protein adopts the expected left-handed four-helical bundle with up-up-down-down connectivities previously observed for IL-4 and similar cytokines. The four helical regions correspond to residues 6-22 (α_A), 43-52 (α_B), 59-70 (α_C), and 92-108 (α_D). The observed angles and axial separation between the four antiparallel helical pairs, α_A-α_C, α_C-α_B, α_B-α_D and α_D-α_A, are -161.7° and 11.3 Å, -147.7° and 9.2 Å, -165.1° and 12.7 Å, and -150.3° and 9.8 Å, respectively. The corresponding values between the two parallel helical pairs, α_A-α_B and α_C-α_D, are 37.0° and 16.4 Å, and 33.4° and 14.2 Å, respectively. In addition, a short β-sheet region was observed in the IL-13 structure that corresponds to residues 33-35 (β_1) and 89-91 (β_2). Additionally, distinct C^β chemical shifts (~42 ppm) for three Cys residues confirmed the presence of two disulfide bonds in the IL-13 structure. The C^β chemical shift for C29

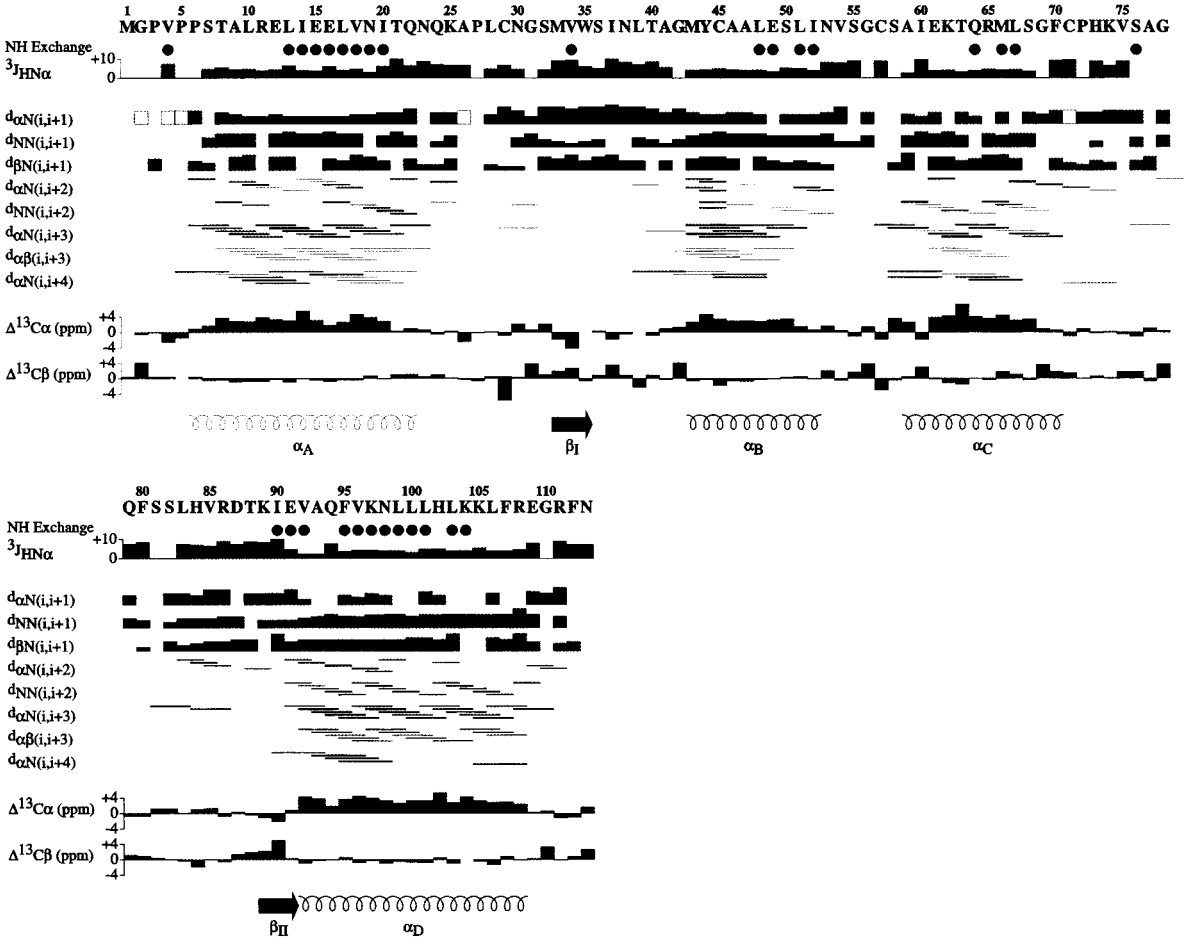

Figure 2. Summary of the sequential and medium-range NOEs involving the NH, H^α and H^β protons, the amide exchange and $^3J_{HN\alpha}$ coupling constant data, and the $^{13}C^\alpha$ and $^{13}C^\beta$ secondary chemical shifts observed for IL-13 with the secondary structure deduced from these data. The thickness of the lines reflects the strength of the NOEs. Amide protons still present after exchange to ^2H_2O are indicated by filled circles. The open boxes on the same line as the $H^\alpha(i)$-NH($i+1$) NOEs represent the sequential NOEs between the H^α proton of residue i and the $C^\delta H$ proton of the $i+1$ proline residue and is indicative of a *trans* proline residue.

Table 1. Structural statistics and atomic r.m.s. differences

A. *Structural statistics*		
r.m.s. deviations from experimental distance restraints (Å)[a]		
All (2248)	0.014 ± 0.002	0.016
Interresidue sequential ($\|i-j\|=1$) (624)	0.011 ± 0.004	0.012
Interresidue short-range ($1<\|i-j\|<5$) (607)	0.015 ± 0.003	0.018
Interresidue long-range ($\|i-j\|>5$) (530)	0.016 ± 0.002	0.021
Intraresidue (437)	0.007 ± 0.004	0.005
H-bonds (50)[b]	0.031 ± 0.006	0.026
r.m.s. deviation from exptl dihedral restraints (deg.) (299)[c,d]-	0.221 ± 0.053	0.186
r.m.s. deviation from exptl C^{α} restraints (ppm) (104)	0.95 ± 0.03	0.94
r.m.s. deviation from exptl C^{β} restraints (ppm) (101)	0.78 ± 0.04	0.78
r.m.s. deviation from $^3J_{NH\alpha}$ restraints (Hz) (96)	0.61 ± 0.02	0.58
F_{NOE} (kcal mol^{-1})[d]	22.3 ± 5.9	28.5
F_{tor} (kcal mol^{-1})[d]	0.95 ± 0.46	0.64
F_{repel} (kcal mol^{-1})[d]	22.5 ± 2.1	14.4
$F_{L\text{-}J}$ (kcal mol^{-1})[e]	−423 ± 8	−408
Deviations from idealized covalent geometry		
Bonds (Å) (1783)	0.003 ± 0	0.004
Angles (deg.) (3240)	0.455 ± 0.011	0.523
Impropers (deg.) (901)[f]	0.437 ± 0.039	0.396
PROCHECK[g]		
Overall G-factor	0.19 ± 0.02	0.15
Residues in most favorable region of Ramachandran plot (%)	90.5 ± 1.4	89.9
Residues in disallowed region of Ramachandran plot (%)	0.0 ± 0.0	0.0
H-bond energy	0.85 ± 0.06	0.90
Number of bad contacts/100 residues	2.6 ± 1.5	1.8

B. *Atomic r.m.s. differences (Å)*

	Residues 1-113		Secondary structure[h]		Ordered side-chain
	Backbone atoms	All atoms	Backbone atoms	All atoms	All atoms
⟨SA⟩ *versus* $\overline{SA}$	0.43 ± 0.04	0.81 ± 0.06	0.22 ± 0.03	0.65 ± 0.06	0.47 ± 0.04
⟨SA⟩ *versus* $(\overline{SA})_r$	0.45 ± 0.04	0.90 ± 0.07	0.24 ± 0.03	0.73 ± 0.08	0.51 ± 0.04
$(\overline{SA})_r$ *versus* $\overline{SA}$	0.15	0.38	0.10	0.32	0.20

The notation of the structures is as follows: ⟨SA⟩ are the final 30 simulated annealing structures; $\overline{SA}$ is the mean structure obtained by averaging the coordinates of the individual SA structures best fit to each; and $(\overline{SA})_r$ is the restrained minimized mean structure obtained by restrained minimization of the mean structure $\overline{SA}$.[50] The number of terms for the various restraints is given in parentheses.

[a] None of the structures exhibited distance violations greater than 0.2 Å or dihedral angle violations greater than 1°.

[b] For backbone NH-CO hydrogen bond there are two restraints: $r_{NH\text{-}O} = 1.5\text{-}2.3$ Å and $r_{N\text{-}O} = 2.5\text{-}3.3$ Å. All hydrogen bonds involve slowly exchanging NH protons.

[c] The torsion angle restraints comprise 104 ϕ, 105 ψ, 66 $\chi1$, and 24 $\chi2$ restraints.

[d] The values of the square-well NOE (F_{NOE}) and torsion angle (F_{tor}) potentials (cf. equations (2) and (3) in Clore *et al.*[51]) are calculated with force constants of 50 kcal mol^{-1} Å^{-2} and 200 kcal mol^{-1} rad^{-2}, respectively. The value of the quartic van der Waals repulsion term (F_{rep}) (cf. equation (5) in Nilges *et al.*[42]) is calculated with a force constant of 4 kcal mol^{-1} Å^{-4} with the hard-sphere van der Waals radius set to 0.8 times the standard values used in the CHARMM[52] emperical energy function.[42,50,53]

[e] $E_{L\text{-}J}$ is the Lennard-Jones-van der Waals energy calculated with the CHARMM emperical energy function and is not included in the target function for simulated annealing or restrained minimization.

[f] The improper torsion restraints serve to maintain planarity and chirality.

[g] These were calculated using the PROCHECK program.[19]

[h] The residues in the regular secondary structure are 6-22(α_A), 43-52(α_B), 59-70(α_C), 92-108(α_D), 33-35(β_I) and 89-91(β_{II}).

was anomalous, where the chemical shift (34 ppm) was between typical values for both oxidized and reduced forms. The further identification of the C29-C57 and C45-C71 disulfide bonds was determined by distinct intermolecular NOEs that were identified during the IL-13 structure calculation. In particular, C29 H^{α} to C57 H^{β}, C29 H^{β} to C57 H^{β} NOEs and C45 H^{α} to C71 H^{β}, C45 H^{β} to C71 H^{β} NOEs defined the C29-C57 and C45-C71 disulfide bonds, respectively.

An interesting observation for the IL-13 structure is the presence of chemical shift heterogeneity in the 2D ^{1}H-^{15}N HSQC spectra for residues in the structural vicinity of C29. In addition to residues sequential to C29 and C57, A93 and residues sequential to A93 exhibited multiple ^{1}H-^{15}N HSQC peaks. Except for the backbone NH resonance assignments, the remainder of the spin-system chemical shifts assignments for these residues were essentially identical. More importantly, the 3D ^{15}N-edited NOESY spectra exhibited identical NOE patterns and relative intensities for the multiple backbone NH diagonal peaks. Therefore, the chemical shift multiplicity observed in the 2D ^{1}H-^{15}N HSQC spectra suggests a local conformational heterogeneity in the vicinity of C29,

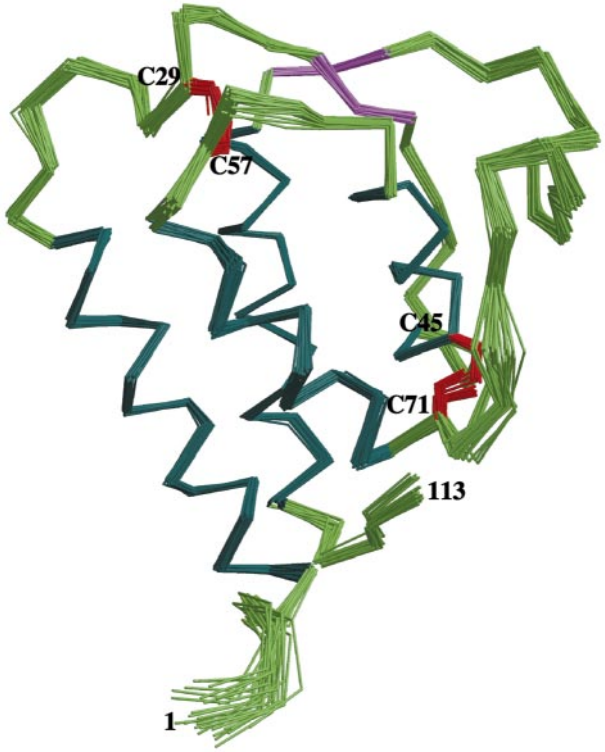

Figure 3. Best-fit superposition of the backbone atoms (N, C, C′) of the 30 best structures determined for IL-13 for residues 1-113 colored by secondary structure, where helices are dark green, β-sheet is magenta and unstructured regions are light green. The two disulfide bonds are labeled and colored red.

where the IL-13 structural change is within the resolution of the structure and the limits of detection for an NOE intensity change. A probable source for the structural heterogeneity is the presence of multiple conformations for the side-chain dihedral angles that comprise the C29-C57 disulfide bond. The C^{α}-C^{α} distance separation for the two cysteine residues involved in a disulfide bond are dependent directly on the side-chain dihedral angles.[20] A distance range of 4.4 to 6.8 Å for the C^{α}-C^{α} separation is observed for typical values of dihedral angles observed in a disulfide bond, but distance changes of only 0.1-0.2 Å is common between pairs of side-chain conformations. Most likely, a smaller distance change is the source of the heterogeneity present in IL-13, where the different side-chain conformations result in C29 being slightly closer to either C57 or A93. The conformational heterogeneity centered on C29 may also explain the anomalous C^{β} chemical shift for this residue.

Another feature of the IL-13 structure is the presence of three long loops connecting the four helices. The shortest loop connects helices α_B and α_C and comprises residues N53 to S58. The two long overhand connections are comprised of residues N23 to G42, which connects helices α_A with α_B, and residues C71 to E91, which connects α_C with α_D. These loops come in close contact to form the short β-sheet. Additionally, the C29-C57 disulfide bond connects the AB loop to the BC loop. The combination of the short β-sheet and the disulfide bond results in regions of these loops being relatively well defined. Further stability of the long loops occurs from long-range intermolecular NOEs that result in packing of parts of the loop against the helical bundle.

An another interesting feature of the IL-13 structure is the location of the C45-C71 disulfide bond, which effectively connects the N terminus of α_B with the C terminus of α_C. Since the α_B and α_C helices are also connected by the short BC loop, which is further stabilized by the C29-C57 disulfide bond, the orientation of the α_B and α_C helices is defined extensively by covalent connectivity. The end result is a closed loop connecting the α_B and α_C helices.

Comparison of the IL-13 and IL-4 solution structures

An abundance of structural information for IL-4 has been determined by both NMR and X-ray crystallography, where a reasonable consensus was obtained for the IL-4 structure.[21] Therefore, a single solution structure of IL-4 (PDB ID: 1BBN) was used to simplify the comparison between the solution structure of IL-13 with IL-4.[10,11] Ribbon diagrams for both the IL-13 and IL-4 restrained minimized solution structures are shown in Figure 4. While the overall folding topology of the two proteins is quite similar, there are obvious distinctions between the two structures. A primary distinction is the overall size difference between the two proteins. IL-4 contains a total of 129 residues compared to 113 for IL-13. This results in the extension of the IL-4 structure by ~12 Å along the long axis relative to IL-13. Consistent with the overall size difference are variations in the helix lengths between the IL-4 and IL-13 structures. The length of the four helices in IL-4 corresponds to 17, 23, 26 and 16 residues for helices α_A, α_B, α_C and α_D, respectively. Conversely, in IL-13 helices α_A, α_B, α_C and α_D have lengths of 17, 10, 12 and 17 residues, respectively. Clearly, the most pronounced distinction is between helices α_B and α_C, where the IL-4 helices are more than double the length of IL-13. Interestingly, a similar difference in the loop regions between the helices was not seen. The length of the AB, BC and CD loops between IL-4 and IL-13 are identical or nearly identical, where the loops in IL-13 are longer by one or two residues. Similarly, the length of the short β-sheet that comprises part of loops AB and CD are essentially identical. Another distinction between the two protein structures is the number and location of the disulfide bonds. IL-4 has a total of three disulfide bonds that connect the N and C terminus (C3-C127), the AB and BC loops (C24-C64), and helix α_B to loop CD (C46-C99). Conversely, IL-13 contains only two disulfide bonds that connect the AB

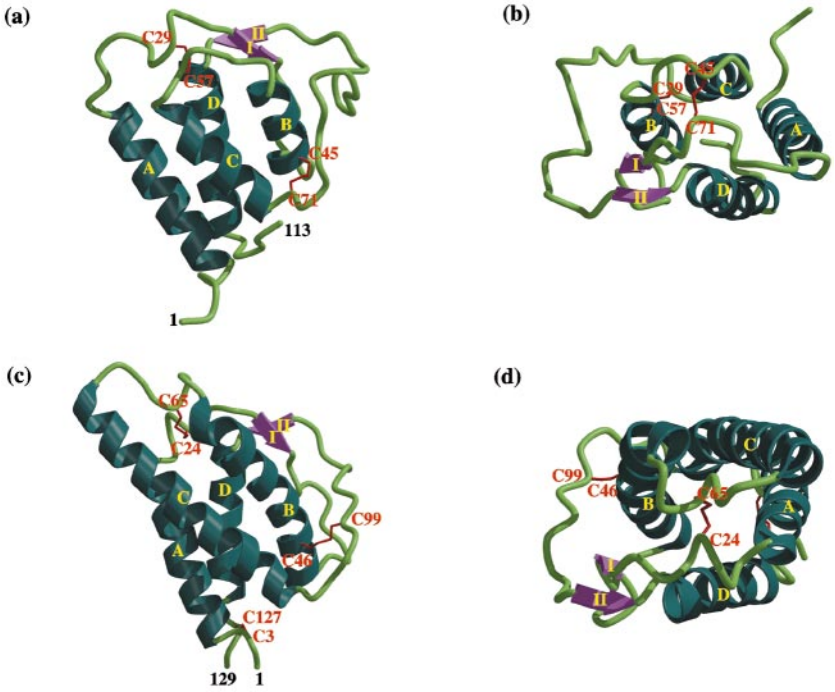

Figure 4. (a) Ribbon diagram of the NMR structure of IL-13 colored by secondary structure (same view as Figure 2). (c) Ribbon diagram of the NMR structure of IL-4 (1BBN).[10,11] The view is the same as that of IL-13 based on the alignment of the common secondary structure elements and disulfide bonds. (b) and (d) Top view of the IL-13 and IL-4 NMR ribbon diagram, respectively, illustrating the helix packing and orientation. The secondary structure elements and cysteine residues involved in disulfide bonds are labeled and colored similar to those in Figure 2.

and BC loops (C29-C57) and helix α_B to helix α_C (C45-C71).

A 25 % sequence homology exists between IL-13 and IL-4; however, optimal superposition of the two proteins is determined mainly by alignment of shared secondary structure elements. An overlay of the IL-13 and IL-4 solution structures based on the common secondary structure elements and Cys residues yielded a backbone r.m.s. of 1.44 Å. The sequential alignment based on the shared secondary structure elements and Cys residues along with the overlay of the backbone atoms for IL-13 with IL-4 is illustrated in Figure 5. In general, there is a good agreement in the superposition between the IL-13 and IL-4 structures, including the loop regions. Nevertheless, there exist some distinct differences between the two proteins in the relative orientations and packing of the four-helix bundle, where α_B and α_D exhibit the largest changes. This is exemplified by an observed 20° difference in the interhelical angle between helices α_B-α_D and changes in opposite directions in the axial separation for helices α_A-α_B and α_C-α_D. The α_A-α_B axial separation decreases from 16.4 Å to 12.6 Å between IL-13 and IL-4, respectively. Conversely, the α_C-α_D axial separation increases from 14.2 Å to 16.7 Å between IL-13 and IL-4. Since α_B in IL-13 is the shortest helix and half the length of α_B in IL-4, the observed structural changes may be attributed to this change in helix length. Furthermore, the relative orientation of α_B in IL-13 is also defined by the disulfide bonds at both the N and C-terminal ends of the helix. Comparison of IL-13 with IL-4 indicates that only a partial spatial alignment of the conserved cysteine residues occurs, further contributing to the perturbation in α_B. There is a good agreement with the relative orientation of C45 from IL-13 with C46 from IL-4. To a lesser extent, the positioning of C29 from IL-13 agrees with C24 from IL-4. But, there is essentially no correlation between the other members of the disulfide pairs. This difference results from the shorter α_B and α_C helices in IL-13 and the fact that C99 resides within the CD loop in IL-4 compared to C71 being located in helix α_C for IL-13. Despite the highlighted differences between IL-13 and IL-4, it is important to stress that the overlap of the protein folds for the two proteins is quite similar.

Implication for IL-13 receptor binding

The recent X-ray crystal structure of IL-4 complexed to the IL-4 receptor α chain has provided insight into cytokine-receptor interactions. Furthermore, an abundance of prior mutational work provides additional information pertaining to the characteristics of the cytokine-receptor interactions. A strong overlap in functionality exists for IL-13 and IL-4 that is further exemplified by the fact that both receptors contain the same IL-4α chain. Therefore, the combination of the observed similarity in the protein folds, mutational data and the IL-4/receptor complex provides a framework to investigate the interaction of IL-13 with its receptor.

A combination of mutational and kinetic analysis has identified a distinct site on the IL-4 structure associated with IL-4Rα binding and a second site associated with signaling through the γ_c chain.[15–17] The IL-4Rα binding site on IL-4 is associated with amino acid residues that comprise a surface formed by helices A (I5, E9, T13) and C (K77, R81, K84, R85 R88, N89, W91). The second

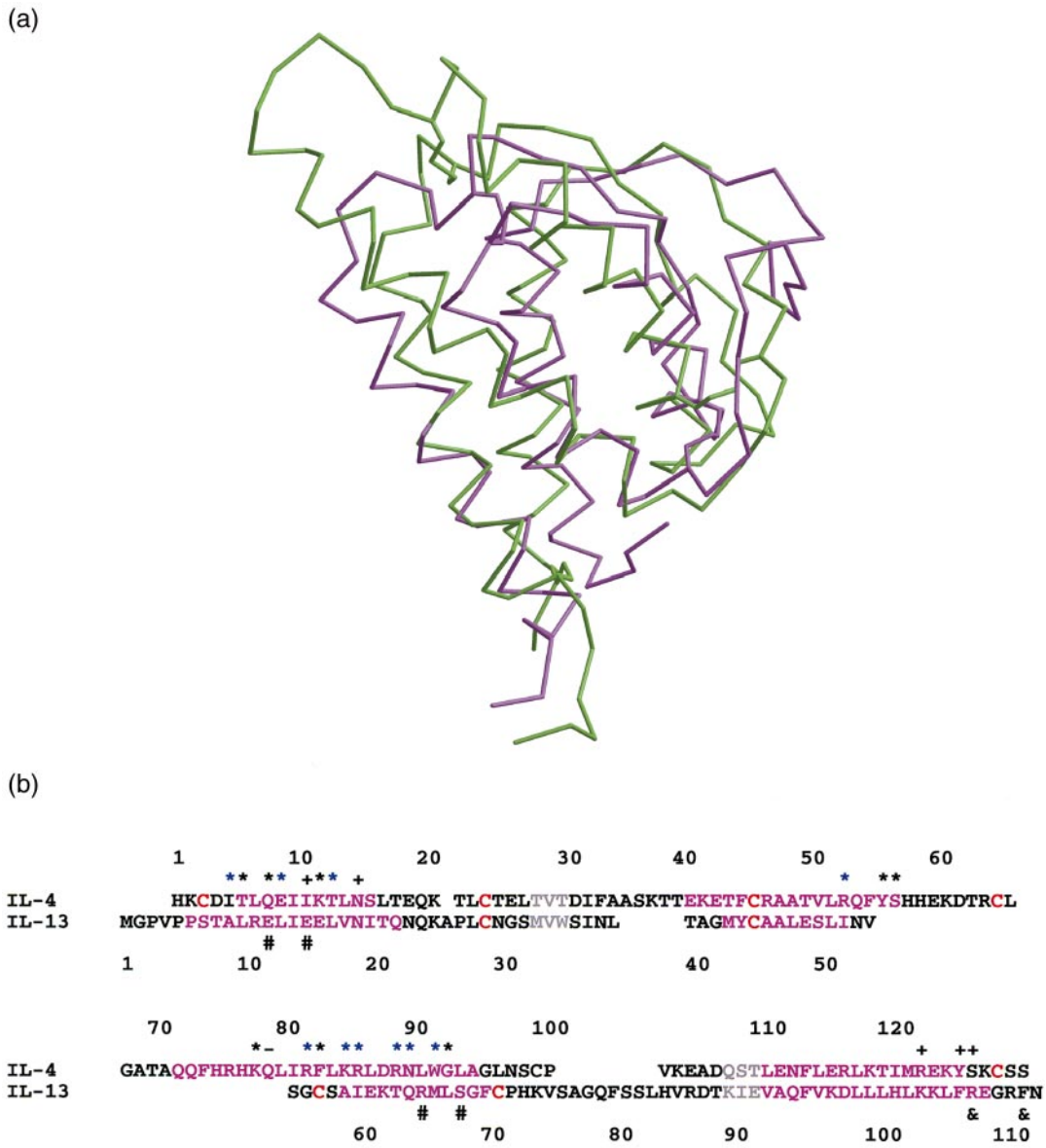

Figure 5. (a) Best-fit superposition of the backbone atoms (N, C, C′) of the IL-13 (magenta) and IL-4 (green, PDB ID: 1BBN) restrained minimized average NMR structures[10,11] (b) The sequence alignment of IL-13 with IL-4 based on the common secondary structure elements and disulfide bonds. Residues assigned to an α-helix are colored pink, to a β-strand are colored gray and the cysteine residues are colored red. The IL-4 mutational data and residues involved in the IL-4Rα binding site based on the IL-4/IL4Rα X-ray structure (PDB ID:1IAR)[18] are indicated on top of the sequence. The IL-13 mutational data are indicated on the bottom of the sequence. IL-4 residues involved in the IL-4Rα and the γ_C binding sites identified by mutational analysis are labeled with (*) and (+), respectively. If the mutational data correlate with the binding interface defined by the IL-4/IL4Rα X-ray structure, the label is colored blue. IL-4 residues identified as part of the IL-4Rα binding site from the X-ray structure without corresponding mutational data are labeled with (−). IL-13 residues involved in the IL-4Rα and the IL-13 binding chain binding sites identified by mutational analysis are labeled with (#) and (&), respectively. The IL-4 sequence numbering is on top and the IL-13 sequence numbering is on the bottom.

site associated with signaling through the γ_c chain corresponds to residues in helices A (I11, N15) and D (R121, Y124, S125). Similar mutational work on IL-13 that alters its reactivity to IL-13R has identified amino acids in helices A (E12, E15), C (R65, S68) and D (R108, F112), based on the predicted secondary structure for IL-13.[22,23] The results of the mutational analysis were mapped onto a GRASP surface for both IL-4 and IL-13 (Figure 6(a) and (c)). This analysis identifies the potential IL-13 binding chain and IL-4Rα binding sites on IL-13, which are consistent with the IL-4 binding sites.

The X-ray structure of IL-4 complexed to IL-4Rα confirmed the previous mutational data in identifying the α-chain binding site on IL-4, while further elucidating the specifics of the protein-receptor

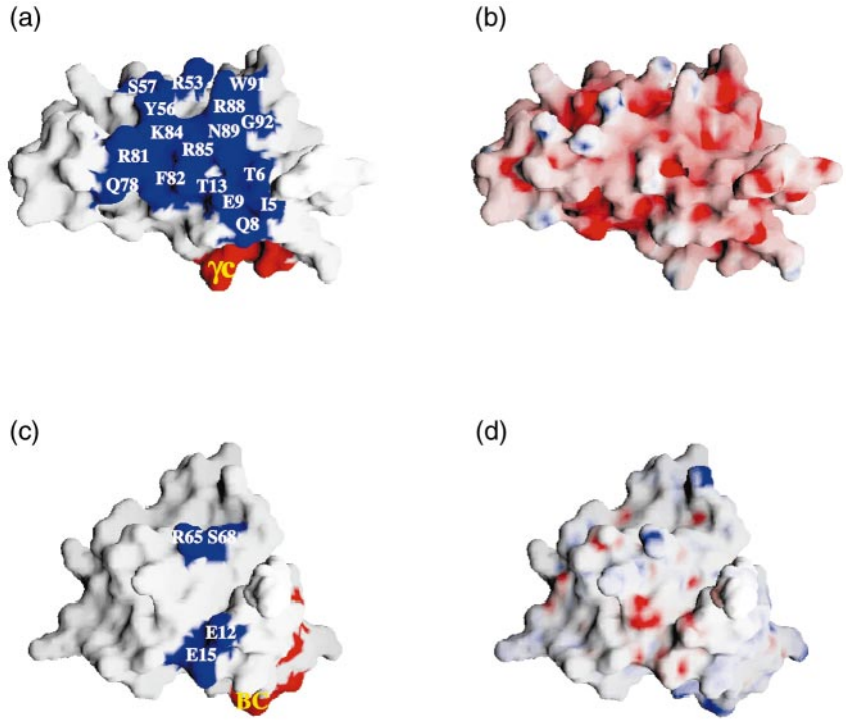

Figure 6. (a) and (c) GRASP molecular surface of the IL-4 and IL-13 NMR structures, respectively, where residues identified from mutational analysis that correlate with IL-4Rα affinity are colored blue. Residues proposed to interact with either the γ_C or IL-13 binding chain (BC) are colored red. Residues in the IL-4Rα binding sites that were mutated are labeled. (b) and (d) The same molecular surface and view for the IL-4 and IL-13 structures, respectively, colored by electrostatic potential, where red corresponds to negative, blue to positive and white to neutral.

interaction.[18] The face of helices α_A and α_C from IL-4 are almost perpendicular to the L-shaped structure of IL-4Rα. Contact residues from IL-4 are predominantly polar and charged, while the complementary receptor epitope is composed of clusters of polar residues surrounded by hydrophobic residues. Three distinct clusters of residues are described where E9 and R88 from IL-4 are focal points in clusters I and II, respectively, where these residues are involved in hydrogen bonds and ionic bonds with numerous IL-4Rα residues. A number of additional IL-4 residues proximal to E9 and R88 complete the IL-4-receptor interface. The third cluster is described as primarily an electrostatic interaction that does not contribute significantly to the binding affinity, but facilitates complex formation. An overlay of the backbone atoms of IL-13 with IL-4 based primarily on a correlation of secondary structure elements provided a mechanism to establish a structure-based sequence alignment. This structure-based sequence alignment of IL-13 with IL-4 is shown in Figure 4, where both the mutational data and the key contact residues from the IL-4/receptor X-ray structure are summarized. Again, there is a clear consistency between the IL-4 mutational and structure contact data, where the IL-13 mutational data correlate well with this information. The overlay of the IL-13 structure with IL-4 may then be used in a similar manner to create a model of IL-13 complexed with IL-4Rα.

By creating a best-fit superposition of IL-13 with IL-4 in the IL-4/IL-4Rα complex, a simple model of IL-13 complexed with IL-4Rα is obtained. An overlay of the IL-13 NMR structure with IL-4 from the IL-4/receptor X-ray structure based on the common secondary structure elements and Cys residues yielded a backbone r.m.s. of 1.55 Å. Additional refinement of the IL-13/IL-4Rα complex was limited to minimization of the IL-13 side-chain conformations to remove obvious steric clashes between IL-13 and IL-4Rα. The IL-13/IL-4Rα model is illustrated in Figure 7. It is readily apparent that the general interaction of IL-13 closely mimics the IL-4/IL-4Rα complex. Particularly, helices α_A and α_C pack approximately perpendicular against IL-4Rα (Figure 7(a)). Furthermore, the framework of the IL-13 side-chain interactions with IL-4Rα mimics the network of interactions observed in the IL-4/IL-4Rα complex. In particular, E12 from IL-13 is positioned to mimic the bonding network of E9 from IL-4 with Y13, Y183 and S70 from IL-4Rα (Figure 7(b)). Similarly, R65 from IL-13 is reasonably positioned to form a potential salt-bridge with D72 from IL-4Rα (Figure 7(c)). This interaction is comparable to the interaction of R88 from IL-4 with D72 from IL-4Rα. Distinctions between the IL-13/IL-4Rα model relative to the IL-4/IL-4Rα X-ray structure becomes apparent when comparison of the binding network that complement the E12 and R65 interaction with IL-4Rα is made. By reference to IL-4, residues proximal to E12 that are predicted to interact with IL-4Rα consist of IL-13 residues A9, E15, E16 and M66. These residues would correlate with T6, K12, T13 and N89 from IL-4 and interact with S70, Y183, Y127 and A71, respectively (Figure 7(b)). Correspondingly, residues near R65 that are predicted to bind IL-4Rα comprise IL-13 residues I52, Q64 and M66 which correlate with IL-4 residues R53, N89 and W91. These IL-4 residues were shown to interact

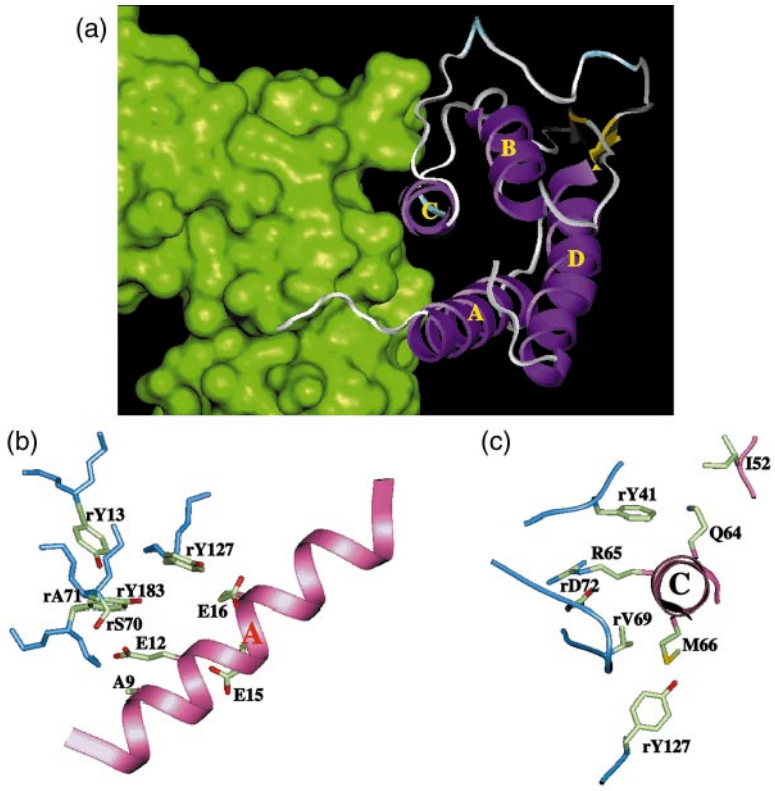

Figure 7. (a) IL-13/IL-4Rα model based on the IL-4/IL-4Rα X-ray structure (PDB ID:1IRA).[18] IL-13 replaced IL-4 in the IL-4/IL-4Rα X-ray structure by overlaying IL-13 onto IL-4 based on the common secondary structure elements and cysteine residues (see Figure 4). IL-4Rα is shown as a molecular surface (green) and IL-13 as a ribbon diagram colored by secondary structure, where the helices are colored purple and the β-sheets are colored yellow. Only the IL-13/IL-4Rα interface is illustrated. The secondary structure elements are labeled. (b) Expanded view of the IL-13/IL-4Rα binding site indicating the interaction with helix α_A from IL-13. (c) Expanded view of the IL-13/IL-4Rα binding site illustrating the interaction with helix α_C from IL-13. The side-chains for critical residues based on the IL-4/IL-4Rα X-ray structure and mutational data are shown and labeled. Residues from IL-4Rα are labeled with the prefix r. The side-chains are colored by element type, the backbone atoms for IL-13 and IL-4Rα are colored magenta and blue, respectively.

with F41 and V69 from IL-4Rα (Figure 7(c)). While some comparable interactions are potentially present in the IL-13/IL-4α models, these interactions are clearly not optimal. Also, there exist some polarity or charge changes that would be predicted to have a detrimental affect on the affinity of IL-13 with IL-4Rα. This is evident by comparison of the GRASP surfaces for IL-4 and IL-13 colored by electrostatic potential. A distinct surface is presented to IL-4Rα by the two proteins, where IL-4 presents a relatively higher negatively charged surface compared to IL-13 (Figure 6(b) and (d)). Conversely, the IL-13 surface is more hydrophobic compared to IL-4 with some positive charge characteristics. This analysis implies that while some key interactions consistent with the IL-4/IL-4Rα complex are present, the IL-13/IL-4Rα model predicts that some re-arrangement of the IL-13 interaction with IL-4Rα is required to optimize the secondary interactions and accommodate the residue substitutions between IL-13 and IL-4.

The apparent sub-optimal interface between IL-13 and IL-4Rα based on the IL-4/IL-4Rα complex appears consistent with both the experimental affinity of IL-13 with IL-4Rα and the assembly mechanism of IL-4 with IL-4R. A sequential order of binding of IL-4 to IL-4R has been proposed.[24,25] First, IL-4 binds the IL-4Rα chain with high affinity ($K_d = 20$-300 pM). The resulting complex then recruits the common γ_C chain to form the signaling heterodimer. Upon complex formation with IL-4Rα chain, IL-4 incurs a conformational change localized in the putative γ_C chain binding site.[15–18] Presumably, the observed IL-4 conformational change is required to bind the γ_C chain binding. A similar mechanism appears consistent with the interaction of IL-13 with its receptor.

IL-13 does not bind IL-4R or the IL-4Rα chain in the absence of the IL-13 binding chain,[26] but binds to the IL-13 binding chain (IL-13Rα1) with relatively high affinity ($K_d \sim 4$ nM). Following the sequential binding mechanism proposed for IL-4, IL-13 would appear to first bind the IL-13 binding chain. The resulting complex then recruits the IL-4Rα chain to from the signaling heterodimer. Upon complex formation with the IL-13 binding chain,

IL-13 would presumably incur a conformational change that would allow it to bind IL-4Rα. Again, this conformational change would probably resemble the change observed with IL-4 and result in a subtle re-arrangement in IL-13 helices α_A and α_C. Since the IL-13/IL-4Rα model reveals that the basic interaction network consistent with the IL-4/IL-4Rα is present, presumably only a modest modification in the helical packing would establish a comparable binding interface with IL-4/IL-4Rα complex and improve the affinity of IL-13 with IL-4Rα.

Materials and Methods

The uniform ^{15}N and ^{13}C-labeled 113 amino acid residue IL-13 was obtained as follows. The cDNA encoding the mature secreted portion of IL-13 was reconstructed with silent changes that optimized *Escherichia coli* codon usage and increased the AT content at the 5-prime end. The gene was subcloned into the phage T7-*lac* vector pRSET for expression in *E. coli* BL21(DE3). Growth and expression were at 37 °C in shake flasks with minimal medium supplemented with [^{13}C]glucose and/or ^{15}N-labeled ammonium sulfate. The protein was essentially completely insoluble. Cells were broken with a microfluidizer and insoluble IL-13 was collected and dissolved at about 2 mg/ml in 50 mM Ches (pH 9), 6 M guanidine-HCl,1 mM EDTA, 20 mM DTT. The solution was diluted 20-fold into 50 mM Ches (pH 9), 3 M guanidine-HCl, 100 mM NaCl, 1 mM oxidized glutathione and dialyzed twice against ten volumes of 50 mM Ches (pH 9), 100 mM NaCl and once against ten volumes of 20 mM Mes (pH 6). Following clarification by centrifugation, IL-13 was adsorbed to SP-Sepharose and eluted with a gradient of NaCl in Mes buffer. Final purification was by size-exclusion chromatography in 40 mM sodium phosphate, 40 mM NaCl on Superdex 75.

The NMR samples contained 1 mM IL-13 in a buffer containing 40 mM sodium phosphate (pH 6.0), 2 mM NaN_3, 40 m M NaCl, in either 90 % H_2O/10 % ^2H_2O or 100 % ^2H_2O. All NMR spectra were recorded at 25 °C on a Bruker DRX 600 spectrometer equipped with a triple-resonance gradient probe. Spectra were processed using the NMRPipe software package[27] and analyzed with PIPP.[28]

The assignments of the ^1H, ^{15}N, ^{13}CO, and ^{13}C resonances were based on the following experiments: CBCA (CO)NH, CBCANH, C(CO)NH, HC(CO)NH, HNHB, HNCO, HNHA, HNCA and HCCH-COSY (for reviews, see Bax *et al*.[29] and Clore & Gronenborn[30]). The accuracy of the IL-13 NMR assignments was further confirmed during the structure calculation and by sequential NOEs in the ^{15}N-edited NOESY-HMQC spectra and by NOEs between the β-strands observed in the ^{13}C-edited NOESY-HMQC and ^{15}N-edited NOESY-HMQC spectra.

The present structure is based on the experimental distance and torsional angle restraints determined from the following series of spectra: HNHA,[31] HNHB,[32] HACAHB-COSY,[33] 3D ^{15}N-[34,35] and ^{13}C-edited NOESY.[36,37] The ^{15}N-edited NOESY, and ^{13}C-edited NOESY experiments were collected with 100 ms and 120 ms mixing times, respectively.

The β-methylene stereospecific assignments and χ_1 torsion angle restraints were obtained primarily from a qualitative estimate of the magnitude of $^3J_{\alpha\beta}$ coupling constants from the HACAHB-COSY experiment[33] and $^3J_{N\beta}$ coupling constants from the HNHB experiment.[32] Val γ-methyl stereospecific assignments were made from the relative intensity of intraresidue NH-$C^\gamma H$ and $C^\alpha H$-$C^\gamma H$ NOEs.[38] Leu and Ile χ_2 torsion angle restraints and Leu δ-methyl stereospecific assignments were obtained primarily from ^{13}C-^{13}C-long-range coupling constants[39] and the relative intensity of intra-molecular NOEs.[11] The φ and ψ torsion angle restraints were obtained from $^3J_{NH\alpha}$ coupling constants measured from the HNHA experiment[31] and from chemical shift analysis using the TALOS program.[40] The minimum ranges employed for the φ, ψ, and χ torsion angle restraints were ±30 °, ±50 °, and ±20 °, respectively. The NOEs assigned from the 3D ^{15}N and ^{13}C-edited NOESY experiments were classified into strong, medium, weak and very weak, corresponding to interproton distance restraints where non-stereospecifically assignments were corrected appropriately for center averaging.[41]

The structures were calculated using the hybrid distance geometry-dynamical simulated annealing method of Nilges *et al*.[42] with minor modifications[43] using the program XPLOR,[44] adapted to incorporate pseudopotentials for $^3J_{NH\alpha}$ coupling constants,[45] secondary $^{13}C^\alpha/^{13}C^\beta$ chemical shift restraints,[46] radius of gyration,[47] and a conformational database potential.[48,49] The target function that is minimized during restrained minimization and simulated annealing comprises only quadratic harmonic terms for covalent geometry, $^3J_{NH\alpha}$ coupling constants and secondary $^{13}C^\alpha/^{13}C^\beta$ chemical shift restraints, square-well quadratic potentials for the experimental distance, radius of gyration and torsion angle restraints, and a quartic van der Waals term for non-bonded contacts. All peptide bonds were constrained to be planar and *trans*. There were no hydrogen-bonding, electrostatic, or 6-12 Lennard-Jones empirical potential energy terms in the target function. The radius of gyration can be predicted with reasonable accuracy on the basis of the number of residues using a relationship determined empirically from the analysis of high-resolution X-ray structures.[47] The force constant for the conformational database and radius of gyration potentials were kept relatively low throughout the simulation to allow the experimental distance and torsional angle restraints to be the predominant influences on the resulting structures. The force constant for the NOE and dihedral restraints was 30 times and ten times stronger then the force constants used for the conformational database and radius of gyration potentials, respectively.

Overlay of the IL-13 solution structure with free IL-4 and IL-4 in the IL-4/IL4Rα complex was accomplished with Quanta (Molecular Simulations, Inc., San Diego, CA). Minimization of the IL-13 side-chains to remove steric clashes was accomplished with CHARMM (Molecular Simulations, Inc., San Diego, CA). Measurement of the interhelical angles and axial distances in the IL-13 and IL-4 structures was determined using INTERHLX (Dr Kyoko, University of Toronto).

Data deposition

Atomic coordinates for the 30 final simulated annealing structures and the restrained minimized mean structure and the NMR chemical shift assignments of IL-13 have been deposited in the RCSB Protein Data Bank (PDB ID: 1ijz and 1iko) and the BioMagResBank (BMRB-5004), respectively.

Acknowledgments

The authors thank Chu-Lai Hsiao for molecular biology efforts in the development of the IL-13 construct, and Karl Malakian and Michelle Catino for bacterial fermentation of IL-13 used in preparation of the NMR sample.

References

1. De Vries, J. E. (1998). The role of IL-13 and its receptor in allergy and inflammatory responses. *J. Allergy Clin. Immunol.* **102**, 165-169.
2. Shirakawa, T., Deichmann, K. A., Izuhara, K., Mao, X. Q., Adra, C. N. & Hopkin, J. M. (2000). Atopy and asthma: genetic variants of IL-4 and IL-13 signaling. *Immunol. Today,* **21**, 60-64.
3. Corry, D. B. (1999). IL-13 in allergy: home at last. *Curr. Opin. Immunol.* **11**, 610-614.
4. Finkelman, F. D., Wynn, T. A., Donaldson, D. D. & Urban, J. F., Jr (1999). The role of IL-13 in helminth-induced inflammation and protective immunity against nematode infections. *Curr. Opin. Immunol.* **11**, 420-426.
5. Wills-Karp, M., Luyimbazi, J., Xu, X., Schofield, B., Neben, T. Y., Karp, C. L. & Donaldson, D. D. (1998). Interleukin-13: central mediator of allergic asthma. *Science,* **282**, 2258-2261.
6. Callard, R. E., Matthews, D. J. & Hibbert, L. (1996). IL-4 and IL-13 receptors: are they one and the same? *Immunol. Today,* **17**, 108-110.
7. Gessner, A. & Rollinghoff, M. (2000). Biologic functions and signaling of the interleukin-4 receptor complexes. *Immunobiology,* **201**, 285-307.
8. De Vries, J. E. (1994). Inhibition of IL-4- and IL-13-induced IgE synthesis by an IL-4 mutant protein. *Arb. Paul Ehrlich Inst.* **87**, 275-282.
9. Sprang, S. R. & Bazan, J. F. (1993). Cytokine structural taxonomy and mechanisms of receptor engagement. *Curr. Opin. Struct. Biol.* **3**, 815-827.
10. Powers, R., Garrett, D. S., March, C. J., Frieden, E. A., Gronenborn, A. M. & Clore, G. M. (1992). Three-dimensional solution structure of human interleukin-4 by multidimensional heteronuclear magnetic resonance spectroscopy. *Science,* **256**, 1673-1677.
11. Powers, R., Garrett, D. S., March, C. J., Frieden, E. A., Gronenborn, A. M. & Clore, G. M. (1993). The high-resolution, three-dimensional solution structure of human interleukin-4 determined by multidimensional heteronuclear magnetic resonance spectroscopy. *Biochemistry,* **32**, 6744-6762.
12. Smith, L. J., Redfield, C., Boyd, J., Lawrence, G. M. P., Edwards, R. G., Smith, R. A. G. & Dobson, C. M. (1992). Human interleukin 4. The solution structure of a four-helix bundle protein. *J. Mol. Biol.* **224**, 899-904.
13. Walter, M. R., Cook, W. J., Zhao, B. G., Cameron, R. P., Jr, Ealick, S. E., Walter, R. L. *et al*. (1992). Crystal structure of recombinant human interleukin-4. *J. Biol. Chem.* **267**, 20371-20376.
14. Wlodaver, A., Pavlovsky, A. & Gustchina, A. (1992). Crystal structure of human recombinant interleukin-4 at 2.25 Å resolution. *FEBS Letters,* **309**, 59-64.
15. Wang, Y., Shen, B.-J. & Sebald, W. (1997). A mixed-charge pair in human interleukin 4 dominates high-affinity interaction with the receptor a chain. *Proc. Natl Acad. Sci. USA,* **94**, 1657-1662.
16. Kruse, N., Shen, B. J., Arnold, S., Tony, H. P., Mueller, T. & Sebald, W. (1993). Two distinct functional sites of human interleukin 4 are identified by variants impaired in either receptor binding or receptor activation. *EMBO J.* **12**, 5121-5129.
17. Letzelter, F., Wang, Y. & Sebald, W. (1998). The interleukin-4 site-2 epitope determining binding of the common receptor g chain. *Eur. J. Biochem.* **257**, 11-20.
18. Hage, T., Sebald, W. & Reinemer, P. (1999). Crystal structure of the interleukin-4/receptor a chain complex reveals a mosaic binding interface. *Cell,* **97**, 271-281.
19. Laskowski, R., Rullmannn, J., MacArthur, M., Kaptein, R. *et al*. (1996). AQUA and PROCHECK-NMR: programs for checking the quality of protein structures solved by NMR. *Biomol. NMR,* **8**, 477-486.
20. Richardson, J. S. (1981). The anatomy and taxonomy of protein structure. *Advan. Protein Chem.* **34**, 167-339.
21. Smith, L. J., Redfield, C., Smith, R. A. G., Dobson, C. M., Clore, G. M., Gronenborn, A. M. *et al*. (1994). Comparison of four independently determined structures of human recombinant interleukin-4. *Nature Struct. Biol.* **1**, 301-310.
22. Thompson, J. P. & Debinski, W. (1999). Mutants of interleukin 13 with altered reactivity toward interleukin 13 receptors. *J. Biol. Chem.* **274**, 29944-29950.
23. Oshima, Y., Joshi, B. H. & Puri, R. K. (2000). Conversion of interleukin-13 into a high affinity agonist by a single amino acid substitution. *J. Biol. Chem.* **275**, 14375-14380.
24. Kondo, M., Takeshita, T., Ishii, N., Nakamura, M., Watanabe, S., Arai, K. & Sugamura, K. (1993). Sharing of the interleukin-2 (IL-2) receptor g chain between receptors for IL-2 and IL-4. *Science,* **262**, 1874-1877.
25. Russell, S. M., Keegan, A. D., Harada, N., Nakamura, Y., Noguchi, M. & Leland, P. *et al*. (1993). Interleukin-2 receptor g chain: a functional component of the interleukin-4 receptor. *Science,* **262**, 1880-1883.
26. Zurawski, S. M., Vega, F., Jr, Huyghe, B. & Zurawski, G. (1993). Receptors for interleukin-13 and interleukin-4 are complex and share a novel component that functions in signal transduction. *EMBO J.* **12**, 2663-2670.
27. Delaglio, F., Grzesiek, S., Vuister, G. W., Zhu, G., Pfeifer, J. & Bax, A. (1995). NMRPipe: a multidimensional spectral processing system based on UNIX pipes. *J. Biomol. NMR,* **6**, 277-293.
28. Garrett, D. S., Powers, R., Gronenborn, A. M. & Clore, G. M. (1991). A common sense approach to peak picking in two-, three-, and four-dimensional spectra using automatic computer analysis of contour diagrams. *J. Magn. Reson.* **95**, 214-220.
29. Bax, A., Vuister, G. W., Grzesiek, S. & Delaglio, F. (1994). Measurement of homo- and heteronuclear *J* couplings from quantitative *J* correlation. *Methods Enzymol.* **239**, 79-105.
30. Clore, G. M. & Gronenborn, A. M. (1994). Multidimensional heteronuclear nuclear magnetic resonance of proteins. *Methods Enzymol.* **239**, 349-362.
31. Vuister, G. W. & Bax, A. (1993). Quantitative *J* correlation: a new approach for measuring homonuclear three-bond *J*(HNH. alpha.) coupling constants in

^{15}N-enriched proteins. *J. Am. Chem. Soc.* **115**, 7772-7777.
32. Archer, S. J., Ikura, M., Torchia, D. A. & Bax, A. (1991). An alternative 3D NMR technique for correlating backbone nitrogen-15 with side chain H. beta. resonances in larger proteins. *J. Magn. Reson.* **95**, 636-641.
33. Grzesiek, S., Kuboniwa, H., Hinck, A. P. & Bax, A. (1995). Multiple-quantum line narrowing for measurement of H.alpha.-H. beta. *J* couplings in isotopically enriched proteins. *J. Am. Chem. Soc.* **117**, 5312-5315.
34. Marion, D., Driscoll, P. C., Kay, L. E., Wingfield, P. T., Bax, A., Gronenborn, A. M. & Clore, G. M. (1989). Overcoming the overlap problem in the assignment of proton NMR spectra of larger proteins by use of three-dimensional heteronuclear proton-nitrogen-15 Hartmann-Hahn-multiple quantum coherence and nuclear Overhauser-multiple quantum coherence spectroscopy: application to interleukin 1. beta. *Biochemistry,* **28**, 6150-6156.
35. Zuiderweg, E. R. P. & Fesik, S. W. (1989). Heteronuclear three-dimensional NMR spectroscopy of the inflammatory protein C5a. *Biochemistry,* **28**, 2387-2391.
36. Zuiderweg, E. R. P., McIntosh, L. P., Dahlquist, F. W. & Fesik, S. W. (1990). Three-dimensional carbon-13-resolved proton NOE spectroscopy of uniformly carbon-13-labeled proteins for the NMR assignment and structure determination of larger molecules. *J. Magn. Reson.* **86**, 210-216.
37. Ikura, M., Kay, L. E., Tschudin, R. & Bax, A. (1990). Three-dimensional NOESY-HMQC spectroscopy of a carbon-13-labeled protein. *J. Magn. Reson.* **86**, 204-209.
38. Zuiderweg, E. R. P., Boelens, R. & Kaptein, R. (1985). Stereospecific assignments of proton-NMR methyl lines and conformation of valyl residues in the lac repressor headpiece. *Biopolymers,* **24**, 601-611.
39. Bax, A. & Pochapsky, S. S. (1992). Optimized recording of heteronuclear multidimensional NMR spectra using pulsed field gradients. *J. Magn. Reson.* **99**, 638-643.
40. Cornilescu, G., Delaglio, F. & Bax, A. (1999). Protein backbone angle restraints from searching a database for chemical shift and sequence homology. *J. Biomol. NMR,* **13**, 289-302.
41. Wuthrich, K., Billeter, M. & Braun, W. (1983). Pseudo-structures for the 20 common amino acids for use in studies of protein conformation by measurements of intramolecular proton-proton distance constraints with nuclear magnetic resonance. *J. Mol. Biol.* **169**, 949-961.
42. Nilges, M., Gronenborn, A. M., Bruenger, A. T. & Clore, G. M. (1988). Determination of three-dimensional structures of proteins by simulated annealing with interproton distance restraints. Application to crambin, potato carboxypeptidase inhibitor and barley serine proteinase inhibitor 2. *Protein Eng.* **2**, 27-38.
43. Clore, G. M., Appella, E., Yamada, M., Matsushima, K. & Gronenborn, A. M. (1990). Three-dimensional structure of interleukin 8 in solution. *Biochemistry,* **29**, 1689-1696.
44. Brunger, A. T. (1993). *X-PLOR Version 3.1 Manual,* Yale University, New Haven, CT.
45. Garrett, D. S., Kuszewski, J., Hancock, T. J., Lodi, P. J., Vuister, G. W., Gronenborn, A. M. & Clore, G. M. (1994). The impact of direct refinement against three-bond HN-C. alpha. H coupling constants on protein structure determination by NMR. *J. Magn. Reson. ser. B,* **104**, 99-103.
46. Kuszewski, J., Qin, J., Gronenborn, A. M. & Clore, G. M. (1995). The impact of direct refinement against ^{13}C. alpha. & ^{13}C. beta. chemical shifts on protein structure determination by NMR. *J. Magn. Reson. ser. B,* **106**, 92-96.
47. Kuszewski, J., Gronenborn, A. M. & Clore, G. M. (1999). Improving the packing and accuracy of NMR structures with a Pseudopotential for the radius of gyration. *J. Am. Chem. Soc.* **121**, 2337-2338.
48. Kuszewski, J., Gronenborn, A. M. & Clore, G. M. (1996). Improving the quality of NMR and crystallographic protein structures by means of a conformational database potential derived from structure databases. *Protein Sci.* **5**, 1067-1080.
49. Kuszewski, J., Gronenborn, A. M. & Clore, G. M. (1997). Improvements and extensions in the conformational database potential for the refinement of NMR and X-ray structures of proteins and nucleic acids. *J. Magn. Reson.* **125**, 171-177.
50. Nilges, M., Clore, G. M. & Gronenborn, A. M. (1988). Determination of three-dimensional structures of proteins from interproton distance data by dynamical simulated annealing from a random array of atoms. Circumventing problems associated with folding. *FEBS Letters,* **239**, 129-136.
51. Clore, G. M., Nilges, M., Sukumaran, D. K., Bruenger, A. T., Karplus, M. & Gronenborn, A. M. (1986). The three-dimensional structure of .alpha.1-purothionin in solution: combined use of nuclear magnetic resonance, distance geometry and restrained molecular dynamics. *EMBO J.* **5**, 2729-2735.
52. Brooks, B. R., Bruccoleri, R. E., Olafson, B. D., States, D. J., Swaminathan, S. & Karplus, M. (1983). CHARMM: a program for macromolecular energy, minimization, and dynamics calculations. *J. Comput. Chem.* **4**, 187-217.
53. Nilges, M., Clore, G. M. & Gronenborn, A. M. (1988). Determination of three-dimensional structures of proteins from interproton distance data by hybrid distance geometry-dynamical stimulated annealing calculations. *FEBS Letters,* **229**, 317-324.

Edited by P. E. Wright

(Received 21 February 2001; received in revised form 2 May 2001; accepted 2 May 2001)